

Suppressing dissipation in a Floquet-Hubbard system

Konrad Viebahn, Joaquín Minguzzi, Kilian Sandholzer, Anne-Sophie Walter, Frederik Görg, and Tilman Esslinger*
Institute for Quantum Electronics, ETH Zurich, 8093 Zurich, Switzerland

(Dated: March 13, 2020)

The concept of ‘Floquet engineering’ relies on an external periodic drive to realise novel, effectively static Hamiltonians. This technique is being explored in experimental platforms across physics, including ultracold atoms, laser-driven electron systems, nuclear magnetic resonance, and trapped ions. The key challenge in Floquet engineering is to avoid the uncontrolled absorption of photons from the drive, especially in interacting systems in which the excitation spectrum becomes effectively dense. The resulting dissipative coupling to higher-lying modes, such as the excited bands of an optical lattice, has been explored in recent experimental and theoretical works, but the demonstration of a broadly applicable method to mitigate this effect is lacking. Here, we show how two-path quantum interference, applied to strongly-correlated fermions in a driven optical lattice, suppresses dissipative coupling to higher bands and increases the lifetime of double occupancies and spin-correlations by two to three orders of magnitude. Interference is achieved by introducing a weak second modulation at twice the fundamental driving frequency with a definite relative phase. This technique is shown to suppress dissipation in both weakly and strongly interacting regimes of a driven Hubbard system, opening an avenue to realising low-temperature phases of matter in interacting Floquet systems.

Dissipation emerges when a system is coupled to a large number of degrees of freedom in its environment. In periodically driven systems dissipation thus naturally arises when the low-energy modes are coupled to lossy excited modes by the drive. This presents a formidable challenge to Floquet engineering, in which periodic driving is used to create a host of novel, effectively static Hamiltonians, with ultracold atoms [1–4] and beyond [5–8]. The success of Floquet engineering relies on the existence of a favourable timescale on which a given Floquet Hamiltonian remains valid before heating kicks in and harms the quantum state. Adding interactions to the picture, the effects of unwanted energy absorption is further complicated by a dense excitation spectrum [9–15]. Consequently, the choice of Floquet driving frequency is always a compromise [16]. On the one hand, the Floquet driving frequency should be chosen as high as possible so as to maximise the detuning between the drive and the natural (low-)energy scale of interest [7, 13, 16]. On the other hand, the presence of higher-lying modes of the underlying Hamiltonian, such as energetically higher Bloch bands in an optical lattice [3, 4, 16–24], pose a limit on how high the drive frequency can be. In practice, the dissipative coupling to higher bands, due to tunnelling within the excited band, inhomogeneities, or subsequent excitations to even higher bands, are the limiting factor in many Floquet driving schemes. While tailored lattice potentials can be employed to push excited bands to higher frequencies and keeping the lowest band dispersive [20], a broadly applicable solution to counteract this form of dissipation has so far not been demonstrated in many-body systems in which the excited modes are densely spaced.

In this paper, we study strongly-correlated fermions in an amplitude-modulated optical lattice, i.e. the driven Fermi-Hubbard model, in which the drive couples dissi-

patively to higher Bloch bands. We demonstrate control of dissipation by introducing a second excitation pathway at twice the fundamental driving frequency and tuning the relative phase [25–28] between the two drives to maximise quantum interference.

The starting point for our experiments is an equal spin mixture of 45’000 to 60’000 ultracold potassium-40 atoms loaded in an optical lattice, realising the Fermi-Hubbard model (Fig. 1a). The three-dimensional, hexagonal lattice structure (the y -direction is not shown in Fig. 1a) is characterised by tunnel couplings $(t_x, t_y, t_z)/h = (340, 90, 106)$ Hz [29] and the Hubbard U/h can be tuned to values between -7 kHz and 7 kHz (h is Planck’s constant). Of the lowest two (S -type) bands of the optical lattice the ground band is typically populated by 65% of the atoms. The excited-orbital bands (P, D, \dots) give rise to a multi-band Hubbard model and are not populated in the static case (Fig. 1a).

Periodic driving is introduced via amplitude modulation of the lattice depth in x -direction with the waveform

$$V_{\tilde{x}}(\tau) = V_0 \times [1 + A_\omega \cos(\omega\tau) + A_{2\omega} \cos(2\omega\tau + \varphi)] \quad , \quad (1)$$

leading, predominantly, to time-periodic modulation of the tunnelling energy t_x [29]. In the Floquet framework, the periodic modulation of $t_x(\tau)$ could be re-cast into an effective (static) tunnelling t_{eff} when modulating at resonance with an energy scale of the underlying Hamiltonian [2, 4]. For instance, modulating t resonantly with both a static site-offset and the Hubbard U allows for engineering of anyon-Hubbard models [32]. In general, however, lattice modulation also causes unwanted higher-band excitations, particularly for the large driving amplitudes typically required for Floquet engineering [2, 4, 32]. In particular, the appearance of multi-photon resonances (Fig. 1b) represents a limitation on the choice of Floquet

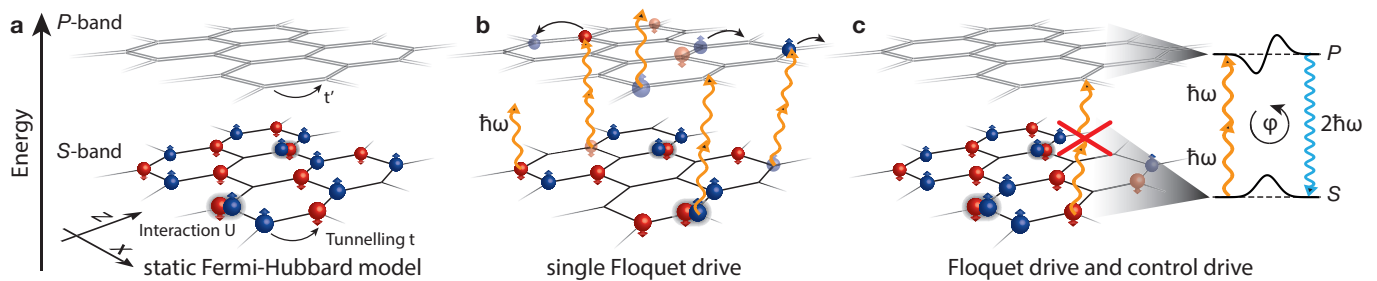


FIG. 1. Two-frequency driving suppresses dissipative coupling to higher bands. (a) Ultracold fermionic atoms in two internal states \uparrow, \downarrow occupy a three-dimensional, hexagonal optical lattice (y -direction omitted for clarity). They are described by the ground-band Fermi-Hubbard model with characteristic energies t (tunnelling) and U (on-site interaction), while energetically higher-lying bands (tunnelling t') are not populated in the absence of periodic driving. Here, only the fifth band is shown, which originates from hybridised (P -)orbitals in x -direction. (b) Periodic driving close to resonance with an inter-band transition leads to dissipation in the ground-band Fermi-Hubbard system, originating from excited-band tunnelling (t'), inhomogeneities, or subsequent excitation to even higher bands. The first relevant resonance is a two-photon process at frequency ω (shown in orange), whereas the single-photon transition is located at 2ω (blue). (c) When applying two driving frequencies simultaneously with matched transition strengths, tuning the relative phase φ coherently enhances or suppresses dissipative coupling to higher bands.

driving frequency and amplitude [16, 18, 22].

We characterise single- and multi-photon resonances experimentally by tuning the Hubbard U to zero and recording the excitation spectrum for two different values of the single-frequency modulation amplitude A_ω (Fig. 2a, $A_{2\omega} = 0$). Here, we modulate the lattice at frequency ω for a duration of 20 ms and record the number of atoms in the ground band (N_{ground}) by counting atoms in Brillouin-zones after band-mapping and time-of-flight [29]. The measurement is in good agreement with a numerical solution to the time-dependent Schrödinger equation, taking into account the non-separable lattice potential in the xz -plane but neglecting any inhomogeneities [29]. Since the modulation is performed on the t_x -bonds, atoms are predominantly excited to the fifth (P -)band which arises from hybridised orbitals in x -direction. Correspondingly, the spectrum in Figure 2a shows pronounced dips in the ground-band population at 24.5 kHz (single-photon resonance) as well as multi-photon resonances at 12.25 kHz (two-photon) and 8.17 kHz (three-photon). When modulating for a varying amount of time, we never observe a revival of the ground band population, moreover, the excitations are accompanied by severe atom loss during the modulation (see below). These observations confirm the dissipative nature of the resonance features.

In the following we outline the strategy to mitigate the previously described dissipation process via destructive interference. Modulation at frequency ω (let us call it the ‘Floquet’ drive) effectively leads to a Rabi-coupling to the higher band [17], which in general can be written as a complex number. Now, the key idea is to add a second modulation at 2ω (the ‘control’ drive) that produces a Rabi-coupling of the same magnitude as the Floquet

drive but with opposite sign, such that both couplings add up to zero, i.e. interfere destructively. Experimentally, we introduce the control drive with amplitude $A_{2\omega}$ and vary the relative phase φ between the two drives (Fig. 2b, $A_\omega = 0.115(2)$, $A_{2\omega} = 0.019(2)$). In the presence of the control drive, the ground band atom number N_{ground} shows a strong dependence on φ , which is direct evidence of phase-only control of the dissipation channel. In particular, N_{ground} peaks at $\varphi = 0.00(1)\pi$, corresponding to a time-reversal-symmetric waveform (Eq. 1) for which both couplings are real-valued but differ by a relative minus sign. This measurement is in good agreement with the theoretical prediction (lines in Fig. 2), as maximal destructive interference leads to a ground band atom number as high as $30.6(8) \times 10^3$, which corresponds to 94% of the static value (black arrow in Fig. 2b). In contrast, a relative phase of π causes depopulation of the ground band with less than 20% of atoms remaining, compared to 43% in the absence of the control drive (red arrow). Fixing the relative phase to $\varphi = 0$ allows us to achieve destructive interference for increasing values of Floquet amplitude A_ω with the optimum control amplitude shifting to larger values, in good agreement with theory, as is shown in Figure 2c. This observation highlights the flexibility of the dissipation control scheme which is not bound to any particular Floquet amplitude. As the single-photon excitation strength is much larger than the two-photon coupling [22], only a weak control amplitude is necessary to achieve control.

Having verified the control technique in the single-particle case, we now investigate the influence of interactions on cancelling the dissipative coupling to higher bands. The many-body state in the driven Fermi-Hubbard model is experimentally characterised by four

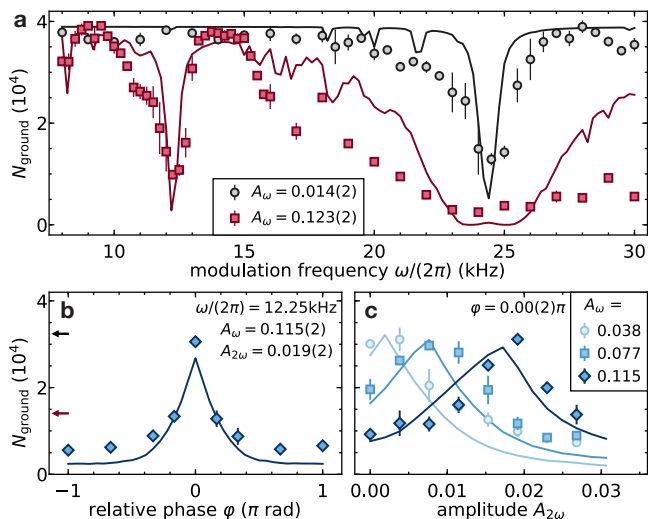


FIG. 2. Optimising dissipation control in the non-interacting regime. (a) Single-frequency excitation spectrum for non-interacting atoms. The data was obtained by modulating the amplitude of the lattice beam in x -direction for 20 ms for two relative strengths A_ω of 0.014(2) (grey circles) and 0.123(2) (red squares). Single- and multi-photon resonance features appear at the S - P inter-band transition at 24.5 kHz and fractions thereof, in agreement with the theoretical calculation (lines) that takes into account the full lattice potential in the xz -plane [29]. (b) Ground band population N_{ground} after 20 ms of two-frequency modulation (Eq. 1) as function of relative phase φ . A matched excitation strength gives rise to a strong dependence on relative phase in agreement with ab-initio theory (lines). The black (red) arrow shows the ground band population in the absence of any drive (in the presence of a single drive at ω). (c) Ground band population at $\varphi = 0$ as function of control amplitude $A_{2\omega}$ for various Floquet amplitudes A_ω . As the Floquet amplitude increases, the optimum control amplitude is shifted to larger values. Error bars to measured data points are the standard error of at least three measurements [29].

different observables, namely total atom number N_{total} , ground band population N_{ground} , double occupancy, and nearest-neighbour spin correlations [29]. In order to maximise our sensitivity, we choose to drive our system resonantly with a two-photon higher-band transition with $\omega/(2\pi) = 12.25$ kHz with an amplitude of $A_\omega = 0.115(2)$, giving rise to a strong dissipative coupling. The driving frequency is chosen to be off-resonant to any static energy scale such that the lowest-band effective Floquet Hamiltonian is equal to the Fermi-Hubbard model, i.e. $t_{\text{eff}} = t_x$. In particular, the Floquet frequency is larger than all probed values of Hubbard U , thus precluding density-assisted tunnelling and creation of double occupancies [20]. In the experiment, we modulate the system for a varying duration τ and different values of Hubbard $|U| < \omega$. This data is then fitted by an exponential decay in order to extract a lifetime. For each

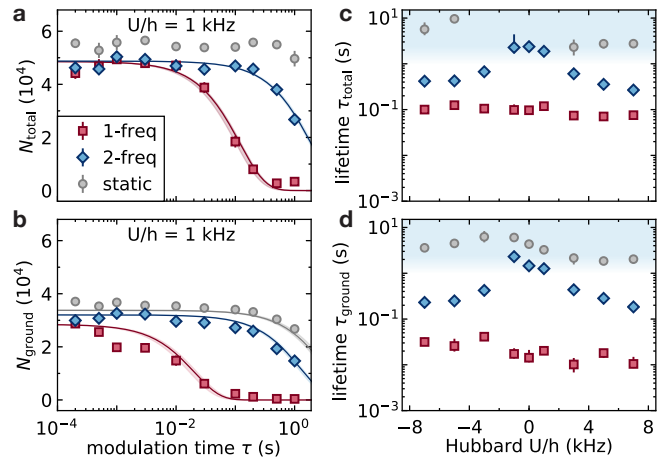


FIG. 3. Effect of interactions on suppressing dissipation. Measured total atom number N_{total} (a) and ground band atom number N_{ground} (b) as function of modulation time, to which an exponential decay is fitted (lines). While a single-frequency drive leads to strong atom loss and de-population of the ground band via higher-band excitations (red points), the presence of the control drive at 2ω (blue) cancels this dissipation mechanism. (c-d) Resulting $1/e$ -lifetimes of the total atom number (τ_{total} , c) and ground band population (τ_{ground} , d) as function of Hubbard U . Since the longest measurement time is 1 s, fitted lifetimes longer than this value can be unreliable (blue shaded area). Data points in (a-b) show the mean and standard error of three individual measurements, whereas the points in (c-d) result from a least-squares fit. The shaded areas in (a-b) and the error bars in (c-d) show the estimated uncertainty of the fitted value via bootstrapping [29].

measurement we compare single-frequency modulation ($A_\omega = 0.115(2)$, $A_{2\omega} = 0$) to the two-frequency driving scheme ($A_\omega = 0.115(2)$, $A_{2\omega} = 0.019(2)$, $\varphi = 0.00(1)\pi$), as well as the static system.

The measured lifetime of both the total atom number τ_{total} and the ground band population τ_{ground} (Fig. 3) show a strongly increased lifetime in the presence of the control drive, compared to the singly-driven case. For weak and intermediate interactions ($|U|/h \lesssim 1.5$ kHz = bandwidth), the lifetime of the ground band atom number (Fig. 3d) is increased by more than two orders of magnitude from 20^{+3}_{-3} ms to $1.3^{+0.1}_{-0.1}$ s at $U/h = 1$ kHz, comparable to the static lifetime. While for strong interactions ($U \gtrsim$ bandwidth) the lifetimes in the two-frequency driving protocol are reduced, compared to the weakly interacting case, applying dissipation control still increases the lifetime by about an order of magnitude. For example, the lifetime of the ground band atom number at strong repulsive interactions ($U/h = 7$ kHz) is increased eighteen-fold from 10^{+4}_{-2} ms to 184^{+27}_{-9} ms, corresponding to more than 2000 Floquet driving cycles.

The improved lifetimes in the band-mapping measurements (Fig. 3) strongly suggest that dissipative coupling to higher bands can be efficiently counteracted by adding

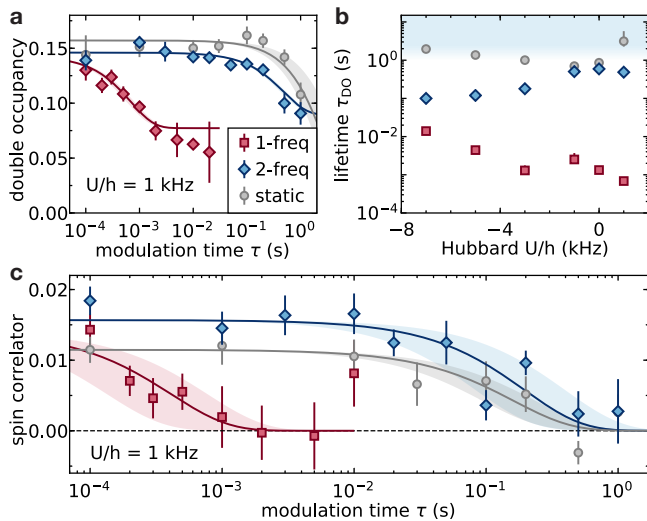


FIG. 4. Suppressing dissipation in the strongly-correlated Fermi-Hubbard model. (a) Measured double occupancy as function of modulation time. Double-occupancy is the fraction of atoms in doubly-occupied lattice sites in the ground band. When applying two-frequency control (blue), the level of double occupancy remains almost unchanged up to 1 s, similar to the static case (grey). (b) Fitted exponential lifetimes of double occupancy τ_{DO} as function of Hubbard U . For weak and intermediate interactions, the control method (blue) restores the lifetime of double occupancy almost to the static value (grey). We restrict this measurement to values of Hubbard $U/h \leq 1$ kHz as the initial value of double occupancy for strong repulsive interactions becomes too low to reliably extract a lifetime. (c) Tracing the nearest-neighbour spin correlator [29] with modulation time for $U/h = 1$ kHz in the presence of the control drive (blue), compared to the single-frequency case (red). The static reference values are plotted in grey. Data points in (a) and (c) show the mean and standard error of at least three and ten individual measurements, respectively, whereas the plotted lifetimes in (b) result from a least-squares fit. The shaded areas in (a,c) and the error bars in (b) show the estimated uncertainty of the fitted value via bootstrapping [29]. Since the longest measurement time is 1 s, fitted lifetimes longer than this value can be unreliable (blue shaded area in b).

the control drive, even for large Hubbard U . However, the single-frequency drive already leads to heating on timescales shorter than the onset of atoms loss in the ground band (10 to 100 ms). In order to investigate this effect, we complement our previous data with measurements of ground-band double occupancy, that is, the fraction of atoms in doubly-occupied sites in the lowest Bloch band [20]. This observable is ideally suited to characterise many-body states in the driven Fermi-Hubbard model and it has been used in the past for an ab-initio comparison of our experiment with non-equilibrium dynamical mean-field theory [33]. In the experiment, we start with a certain level of double occupancy in the static lattice set by the value of U , assum-

ing a thermally equilibrated state [20, 33]. As before, we introduce the modulation for varying amounts of time τ and then freeze the lattice in order to suppress any further dynamics [29]. Atoms on doubly-occupied sites are then associated to Feshbach molecules which experience a shifted zero-point on-site energy. As this on-site energy depends on the Bloch band, we are able to spectroscopically resolve double-occupancies in the ground band; atoms in higher bands are expelled from the trap during the band-mapping ramp while atoms in the lowest band remain trapped [29]. The results of this measurement and the extracted lifetimes (τ_{DO}) are shown in Figure 4a-b. We observe a fast drop in double occupancy ($\tau_{DO} = 0.7^{+0.1}_{-0.1}$ ms for $U/h = 1$ kHz) in the single-frequency case, which precedes the ground band atom loss ($\tau_{DO} \ll \tau_{\text{ground}} = 20^{+3}_{-3}$ ms, Fig. 3d). This observation is consistent with a fast increase in entropy, i.e. heating, which causes the cloud to expand in the trap, resulting in a lower density at the centre of the trap and reduced double occupancy. In stark contrast, the lifetime of double occupancy is increased by up to a factor of hundred when applying two-frequency control. For example, this lifetime exceeds 1 s for $U/h = 1$ kHz which is similar to our static lifetimes, reaching to the limit within which we can reliably extract a lifetime (blue shaded areas). This measurement corroborates the previous results for strongly attractive and weakly repulsive interactions (Fig. 3c-d).

While charge dynamics (e.g., double occupancy) in the Fermi-Hubbard model are governed by t and U , the lowest hierarchy in the system is the spin exchange energy $4t^2/U$. Therefore, spin-correlations are highly susceptible to temperature changes and we thus expect them to vanish quickly in the single-frequency driven case. The experimental data is plotted in Figure 4c which shows that nearest-neighbour spin correlations [29] are indeed destroyed within just a few driving cycles, with a $1/e$ -lifetime of 410^{+360}_{-280} μ s. Remarkably, dissipation control extends the lifetime of nearest-neighbour spin-correlations by three orders of magnitude, to 200^{+200}_{-110} ms which is within measurement error of the static value (160^{+80}_{-70} ms).

In conclusion, we demonstrated how adding a weak harmonic to the fundamental driving frequency can suppress dissipative coupling to higher-lying modes in a driven many-body system, even in the presence of strong interactions. Long lifetimes in strongly-driven, ultracold matter are a prerequisite for realising low-temperature phases in these systems, for example in an anyon-Hubbard model [32]. A natural extension of this scheme employs additional control frequencies to cancel further resonances, in the spirit of pulse-shaping techniques in laser-driven molecular dynamics [34]. Moreover, tuneable couplings to higher bands can be an asset, rather than a nuisance, for instance, in designing novel cooling schemes, not only for optical lattices [17, 35] but also

in condensed matter [36]. More generally, this kind of precisely engineered dissipation is a valuable resource for engineering specific quantum states, particularly in the many-body context [37].

Acknowledgments

We would like to thank J. Léonard, D. Malz, M. Messer, Y. Murakami, P. Werner, and W. Zwerger for discussions and comments on the manuscript. This work was partly funded by the SNF (project nos. 169320 and 182650), NCCR-QSIT, QUIC (Swiss State Secretary for Education, Research and Innovation contract no. 15.0019), and ERC advanced grant TransQ (project no. 742579). K.V. is supported by the ETH Zurich Postdoctoral Fellowship programme.

* esslinger@phys.ethz.ch

- [1] N. Goldman and J. Dalibard, “Periodically Driven Quantum Systems: Effective Hamiltonians and Engineered Gauge Fields,” *Physical Review X* **4**, 31027 (2014).
- [2] Marin Bukov, Luca D’Alessio, and Anatoli Polkovnikov, “Universal high-frequency behavior of periodically driven systems: from dynamical stabilization to Floquet engineering,” *Advances in Physics* **64**, 139–226 (2015).
- [3] Martin Holthaus, “Floquet engineering with quasienergy bands of periodically driven optical lattices,” *Journal of Physics B: Atomic, Molecular and Optical Physics* **49**, 013001 (2016).
- [4] André Eckardt, “Colloquium: Atomic quantum gases in periodically driven optical lattices,” *Reviews of Modern Physics* **89**, 11004 (2017).
- [5] Takashi Oka and Sota Kitamura, “Floquet Engineering of Quantum Materials,” *Annual Review of Condensed Matter Physics* **10**, 387–408 (2019).
- [6] Fenner Harper, Rahul Roy, Mark S. Rudner, and S.L. Sondhi, “Topology and Broken Symmetry in Floquet Systems,” *Annual Review of Condensed Matter Physics* **11** (2020), 10.1146/annurev-conmatphys-031218-013721.
- [7] Pai Peng, Chao Yin, Xiaoyang Huang, Chandrasekhar Ramanathan, and Paola Cappellaro, “Observation of Floquet prethermalization in dipolar spin chains,” arXiv:1912.05799 [cond-mat, physics:quant-ph] (2019), arXiv: 1912.05799.
- [8] Philip Kiefer, Frederick Hakelberg, Matthias Wittmer, Alejandro Bermúdez, Diego Porras, Ulrich Warring, and Tobias Schaetz, “Floquet-Engineered Vibrational Dynamics in a Two-Dimensional Array of Trapped Ions,” *Physical Review Letters* **123**, 213605 (2019).
- [9] Martin Reitter, Jakob Näger, Karen Wintersperger, Christoph Sträter, Immanuel Bloch, André Eckardt, and Ulrich Schneider, “Interaction Dependent Heating and Atom Loss in a Periodically Driven Optical Lattice,” *Physical Review Letters* **119**, 200402 (2017).
- [10] K. Singh, C. J. Fujiwara, Z. A. Geiger, E. Q. Simmons, M. Lipatov, A. Cao, P. Dotti, S. V. Rajagopal, R. Senaratne, T. Shimasaki, M. Heyl, A. Eckardt, and D. M. Weld, “Quantifying and Controlling Prethermal Nonergodicity in Interacting Floquet Matter,” *Physical Review X* **9**, 41021 (2019).
- [11] T. Boulier, J. Maslek, M. Bukov, C. Bracamontes, E. Magnan, S. Lellouch, E. Demler, N. Goldman, and J. V. Porto, “Parametric Heating in a 2D Periodically Driven Bosonic System: Beyond the Weakly Interacting Regime,” *Physical Review X* **9**, 11047 (2019).
- [12] K. Wintersperger, M. Bukov, J. Näger, S. Lellouch, E. Demler, U. Schneider, I. Bloch, N. Goldman, and M. Aidelsburger, “Parametric Instabilities of Interacting Bosons in Periodically Driven 1D Optical Lattices,” *Physical Review X* **10**, 11030 (2020).
- [13] Antonio Rubio-Abadal, Matteo Ippoliti, Simon Hollerith, David Wei, Jun Rui, S. L. Sondhi, Vedika Khemani, Christian Gross, and Immanuel Bloch, “Floquet prethermalization in a Bose-Hubbard system,” arXiv:2001.08226 [cond-mat, physics:quant-ph] (2020), arXiv: 2001.08226.
- [14] Tomotaka Kuwahara, Takashi Mori, and Keiji Saito, “Floquet–Magnus theory and generic transient dynamics in periodically driven many-body quantum systems,” *Annals of Physics* **367**, 96–124 (2016).
- [15] R. Moessner and S. L. Sondhi, “Equilibration and order in quantum Floquet matter,” *Nature Physics* **13**, 424–428 (2017).
- [16] Gaoyong Sun and André Eckardt, “Optimal frequency window for Floquet engineering in optical lattices,” *Physical Review Research* **2**, 013241 (2020).
- [17] Waseem S. Bakr, Philipp M. Preiss, M. Eric Tai, Ruichao Ma, Jonathan Simon, and Markus Greiner, “Orbital excitation blockade and algorithmic cooling in quantum gases,” *Nature* **480**, 500–503 (2011).
- [18] M. Weinberg, C. Ölschläger, C. Sträter, S. Prella, A. Eckardt, K. Sengstock, and J. Simonet, “Multiphoton interband excitations of quantum gases in driven optical lattices,” *Physical Review A* **92**, 043621 (2015).
- [19] Nick Fläschner, Matthias Tarnowski, Benno S. Rem, Dominik Vogel, Klaus Sengstock, and Christof Weitenberg, “High-precision multiband spectroscopy of ultracold fermions in a nonseparable optical lattice,” *Physical Review A* **97** (2018), 10.1103/PhysRevA.97.051601.
- [20] Michael Messer, Kilian Sandholzer, Frederik Görg, Joaquín Minguzzi, Rémi Desbuquois, and Tilman Esslinger, “Floquet Dynamics in Driven Fermi-Hubbard Systems,” *Physical Review Letters* **121**, 233603 (2018).
- [21] Citlali Cabrera-Gutiérrez, Eric Michon, Maxime Arnal, Gabriel Chatelain, Vincent Brunaud, Tomasz Kawalec, Juliette Billy, and David Guéry-Odelin, “Resonant excitations of a Bose Einstein condensate in an optical lattice,” *The European Physical Journal D* **73**, 170 (2019).
- [22] Christoph Sträter and André Eckardt, “Interband Heating Processes in a Periodically Driven Optical Lattice,” *Zeitschrift für Naturforschung A* **71**, 909–920 (2016).
- [23] Ahmet Keleş, Erhai Zhao, and W. Vincent Liu, “Effective theory of interacting fermions in shaken square optical lattices,” *Physical Review A* **95**, 63619 (2017).
- [24] Anton Quelle and Cristiane Morais Smith, “Resonances in a periodically driven bosonic system,” *Physical Review E* **96**, 52105 (2017).
- [25] M. Schiavoni, L. Sanchez-Palencia, F. Renzoni, and G. Grynberg, “Phase Control of Directed Diffusion in a Symmetric Optical Lattice,” *Physical Review Letters* **90**, 94101 (2003).

- [26] Chao Zhuang, Christopher R. Paul, Xiaoxian Liu, Samansa Maneshi, Luciano S. Cruz, and Aephraim M. Steinberg, “Coherent Control of Population Transfer between Vibrational States in an Optical Lattice via Two-Path Quantum Interference,” *Physical Review Letters* **111**, 233002 (2013).
- [27] Linxiao Niu, Dong Hu, Shengjie Jin, Xiangyu Dong, Xuzong Chen, and Xiaoji Zhou, “Excitation of atoms in an optical lattice driven by polychromatic amplitude modulation,” *Optics Express* **23**, 10064 (2015).
- [28] Frederik Görg, Kilian Sandholzer, Joaquín Minguzzi, Rémi Desbuquois, Michael Messer, and Tilman Esslinger, “Realization of density-dependent Peierls phases to engineer quantized gauge fields coupled to ultracold matter,” *Nature Physics* **15**, 1161–1167 (2019).
- [29] See Supplemental Material, which includes Refs. [30, 31], for further experimental details, theoretical calculations, and data analysis.
- [30] D. Greif, T. Uehlinger, G. Jotzu, L. Tarruell, and T. Esslinger, “Short-Range Quantum Magnetism of Ultracold Fermions in an Optical Lattice,” *Science* **340**, 1307–1310 (2013).
- [31] Thomas Uehlinger, Gregor Jotzu, Michael Messer, Daniel Greif, Walter Hofstetter, Ulf Bissbort, and Tilman Esslinger, “Artificial Graphene with Tunable Interactions,” *Physical Review Letters* **111**, 185307 (2013).
- [32] Lorenzo Cardarelli, Sebastian Greschner, and Luis Santos, “Engineering interactions and anyon statistics by multicolor lattice-depth modulations,” *Physical Review A* **94**, 23615 (2016).
- [33] Kilian Sandholzer, Yuta Murakami, Frederik Görg, Joaquín Minguzzi, Michael Messer, Rémi Desbuquois, Martin Eckstein, Philipp Werner, and Tilman Esslinger, “Quantum Simulation Meets Nonequilibrium Dynamical Mean-Field Theory: Exploring the Periodically Driven, Strongly Correlated Fermi-Hubbard Model,” *Physical Review Letters* **123**, 193602 (2019).
- [34] D. G. Kuroda, C. P. Singh, Z. Peng, and V. D. Kleiman, “Mapping Excited-State Dynamics by Coherent Control of a Dendrimer’s Photoemission Efficiency,” *Science* **326**, 263–267 (2009).
- [35] M. Arnal, V. Brunaud, G. Chatelain, C. Cabrera-Gutiérrez, E. Michon, P. Cheiney, J. Billy, and D. Guéry-Odelin, “Evidence for cooling in an optical lattice by amplitude modulation,” *Physical Review A* **100**, 13416 (2019).
- [36] Philipp Werner, Martin Eckstein, Markus Müller, and Gil Refael, “Light-induced evaporative cooling of holes in the Hubbard model,” *Nature Communications* **10**, 5556 (2019).
- [37] Markus Müller, Sebastian Diehl, Guido Pupillo, and Peter Zoller, “Engineered Open Systems and Quantum Simulations with Atoms and Ions,” in *Advances In Atomic, Molecular, and Optical Physics*, Vol. 61 (Elsevier, 2012) pp. 1–80.

Supplemental Material

General preparation

To realize the driven Fermi-Hubbard model, we first prepare a gas of ^{40}K fermionic atoms in the two magnetic sublevels $m_F = -9/2, -7/2$ of the $F = 9/2$ manifold, which is trapped in a harmonic optical dipole trap. We prepare an incoherent spin-balanced mixture of the two spins by performing many radio-frequency sweeps over the transition resonance between the two states. The cloud is then evaporatively cooled to quantum degeneracy at a scattering length of $a = 116(1)a_0$, where a_0 is the Bohr radius. The mean number of atoms in this cloud is $46(2) \cdot 10^3$ at a temperature of $0.09(1)T/T_F$. For strong attractive and weak repulsive interactions we use the $-9/2, -7/2$ mixture, whereas for strong repulsive interactions we use a $-9/2, -5/2$ mixture. The latter is prepared by applying a Landau-Zener sweep to transfer all atoms from the $-7/2$ to the $-5/2$ spin state.

We create a three-dimensional optical lattice by retro-reflecting four beams of wavelength $\lambda = 1064$ nm. The resulting lattice potential perceived by the atoms is:

$$\begin{aligned} V(x, y, z) = & -V_{\bar{X}} \cos^2(k_L x + \theta/2) - V_X \cos^2(k_L x) \\ & -V_{\bar{Y}} \cos^2(k_L y) - V_Z \cos^2(k_L z) \quad (\text{S1}) \\ & -2\alpha \sqrt{V_X V_Z} \cos(k_L x) \cos(k_L z) \cos \varphi_{SL}, \end{aligned}$$

where $k_L = 2\pi/\lambda$ and x, y, z are the three experimental axes. The lattice depths $V_{\bar{X}, X, \bar{Y}, Z}$ are measured in units of the recoil energy $E_R = \hbar^2/2m\lambda^2$, where \hbar is the Planck constant and m the mass of the atoms. Each lattice depth is independently calibrated by modulating its amplitude in the presence of a ^{40}K degenerate Fermi cloud. The visibility $\alpha = 0.958(8)$ is also calibrated using amplitude modulation on a degenerate ^{40}K Fermi cloud, but in an interfering lattice configuration. The phase θ that fixes the geometry of the lattice is set to $\theta = 1.000(2)\pi$, whereas the superlattice phase φ_{SL} is actively stabilized to $0.00(3)\pi$.

Lattice configurations and modulation

The potential from Eq. S2 yields a hexagonal lattice structure, which is characterized by the lowest-band tunnelling rates $t_x, t_{x,\text{inter}}, t_y$ and t_z . We load the atoms from the optical trap into an intermediate lattice within 200 ms, where the tunnelling $t_{x,\text{inter}}$ between dimers remains finite $V_{\bar{X}, X, \bar{Y}, Z}/E_R = [7.89(9), 0.10(2), 9.7(2), 8.2(2)]$. We then linearly ramp up the lattice in 20 ms to a hexagonal configuration with $V_{\bar{X}, X, \bar{Y}, Z}/E_R = [21.0(3), 3.70(4), 9.7(2), 6.81(8)]$ in which the modulation is performed. Here, the resulting tunnelling energies are $[t_x, t_{x,\text{inter}}, t_y, t_z]/\hbar = [340(50), 0.8(1), 90(4), 106(7)]$ Hz, where the inter-dimer

tunnelling $t_{x,\text{inter}}$ is negligibly small.

To implement the periodic drive in the system, we modulate the intensity of the non-interfering, \bar{X} lattice beam by applying a sinusoidal signal to the RF power of an AOM resulting in a modulation of the lattice depth. We obtain a periodically varying lattice depth of the form $V_{\bar{X}}(\tau) = V_{\bar{X}}(1 + A_\omega \sin(\omega\tau))$, where ω corresponds to the ‘Floquet’ driving frequency and A_ω to the relative amplitude of the drive. The lattice modulation leads to a modulation of all Hubbard parameters. However, the influence of the modulation on t_z remains smaller than 13% and that on U smaller than 5%. Such a periodic modulation will also introduce transitions to higher bands. To compensate for these losses, we add an additional ‘control’ contribution to the drive $A_{2\omega} \sin(2\omega\tau + \varphi)$ at twice the frequency. The amplitude and phase of the drive are calibrated by recording the intensity of the lattice beam and performing a fast Fourier-transform on the signal. The remaining systematic deviations are $2^\circ = 0.01\pi$ in the single-frequency driving phase and 0.002 in the amplitude; statistical deviations are smaller than these values. In all measurements presented in the paper the amplitude of the modulation is ramped to its final value within two periods of the fundamental modulation frequency ω and suddenly switched off after the duration of the modulation τ .

Detection methods

The experimental realization of the Fermi-Hubbard model is characterized by four observables: atom number and band population in Figure 3, as well as double occupancy fraction and spin correlations in Figure 4.

Band-mapping detection. The atom number and band population are obtained through a detection method called band-mapping. Directly after the modulation we ramp down the optical lattice slowly enough for the atoms to stay adiabatically in their band but fast enough to avoid redistribution between bands. We thereby map quasi-momentum to real momentum. We do this by an exponential ramp to zero of the lattice depth within 500 μs . After 500 μs we switch off the homogeneous magnetic field and trapping potential and allow for 15 ms time of flight (TOF) to map momentum onto position and thereby resolve the Brillouin zones in real space. We then take an absorption image of the expanded cloud. To assess the distribution of atoms among bands, we divide the image into zones for the different bands and integrate the atomic density in each zone. The centre position of the first Brillouin zone is determined by fitting a Gaussian to a ^{40}K cloud released adiabatically from the trap. The size of the BZ is determined by a separate calibration method where we use a ^{87}Rb condensate and flash the lattice: the $2\hbar k_L$

diffraction peaks yield the edges of the first zone and are corrected by a factor $^{87}/_{40}$ due to the mass difference between ^{87}Rb and ^{40}K .

Stern-Gerlach detection. The measurement of double occupancy fractions and spin-correlations requires another detection method. We release the atoms from the lattice within 100 ms: longer than the $500\ \mu\text{s}$ from the band-mapping to allow for the atoms to redistribute into Gaussian cloud shapes and for atoms in higher bands to be lost from the trap but still short enough to avoid atom loss. Also, these observables require a spin-resolved measurement: to distinguish between the different Zeeman sublevels we apply a short magnetic field gradient which leads to a separation of the spin states during TOF of 8 ms.

Double-occupancy detection. Directly after the modulation we freeze the dynamics through a quench to a deep cubic, 'freeze' lattice $V_{\bar{X},X,\tilde{Y},Z} = [30.6(5), 0.0, 39.9(2), 29.6(8)]$ within $100\ \mu\text{s}$. We then ramp the magnetic field over the $-7/2$, $-9/2$ Feshbach resonance at $B = 202.1\ \text{G}$ and spectroscopically resolve the interaction shift by radio-frequency radiation. As a result, only the atoms sitting in pairs on a lattice site are transferred to another spin state. For the $-7/2, -9/2$ mixture, the atoms in the $-7/2$ are transferred to the $-5/2$ state, while for the $-5/2, -9/2$ mixture, atoms in the $-5/2$ are transferred to the $-7/2$ state. These Zeeman-sublevels are then detected with the previously described Stern-Gerlach method.

Spin-correlations detection. This measurement scheme is described in detail in Ref. [30]. In this paper, we only use the $-7/2, -9/2$ mixture in the spin-correlations measurement. As for the double occupancy detection, we start by ramping the lattice to a cubic 'freeze' lattice. We then eliminate the double occupancies: through consecutive radio-frequency Landau-Zener sweeps we transfer the atoms in the $-7/2$ to the $-3/2$ spin state. In doubly-occupied sites, the $-3/2$, $-9/2$ mixture is very short-lived, and therefore lost from the trap. The remaining single atoms in the $-3/2$ state are transferred back to the $-7/2$ state with two consecutive radio-frequency Landau-Zener sweeps. The nearest-neighbour spin correlator along t_x can be written as

$$\begin{aligned} \text{spin correlator} &= -\frac{1}{N} \sum_{\mathbf{i}} \left[\langle \hat{S}_{\mathbf{i}}^x \hat{S}_{\mathbf{i}+\mathbf{e}_x}^x \rangle + \langle \hat{S}_{\mathbf{i}}^y \hat{S}_{\mathbf{i}+\mathbf{e}_x}^y \rangle \right] \quad (\text{S2}) \\ &= \frac{\text{singlet fraction} - \text{triplet fraction}}{2}, \end{aligned}$$

where $\hat{S}_{\mathbf{i}}$ is the standard vector spin-operator on lattice site \mathbf{i} , the sum runs over all two-site unit cells, \mathbf{e}_x is the unit vector in x direction, and N is the total number of atoms in the ground band. This means full antiferromagnetic correlations along t_x would result

in a spin correlator of one. In order to measure the singlet and triplet fraction, we apply a magnetic field gradient which leads to an oscillation between the two populations. We measure these populations at the two extrema of the oscillations (4.2 ms and 7.8 ms) and infer the spin correlations from the difference. To do so, we ramp the lattice to a checkerboard configuration $V_{\bar{X},X,\tilde{Y},Z} = [0.0, 29.6(5), 39.9(2), 29.6(8)]$ thereby merging adjacent sites with singlets and triplets. Due to the Pauli exclusion principle, the triplets are then converted to one atom in the lowest and another in the first excited band. The singlets on the other hand form double occupancies in the lowest band. These single or double occupancies in the lowest band can be detected with the same method as described previously for double occupancies. To normalize these fractions we determine the total number of atoms N including double occupancies in a separate measurement.

Lifetime and band population fits

To extract a characteristic timescale for the band population transfer and lifetimes for atom number, double occupancy fraction, and spin correlations we use an exponential decay function:

$$P(\tau) = P_0 \exp(-\tau/\tau_P), \quad (\text{S3})$$

where P_0 corresponds to the initial value of the observable, τ is the modulation time, and τ_P the fitted lifetime of the observable. The data points and corresponding error bars as a function of modulation duration correspond to the mean value and standard error from three (Fig. 3a-b, Fig. 4a) to ten (Fig. 4c) independent measurements. The curves in these Figures correspond to the result of fitting Eq. S3 to all measured values.

To obtain an estimate on the uncertainty of the lifetime, we use two different sampling methods. For the double occupancy fraction, atom number and ground band population (Fig. 3 and Fig. 4a-b) we use a method called bootstrapping: we randomly resample values from the measured points and fit the exponential decay function to this data set. For the spin correlations, we assume a normal distribution around the mean measured value for each modulation time. We then sample random values from these distributions and apply an exponential fit to the resulting data set. We repeat both methods 500 times while varying the initialization parameters by plus minus 10%: P_0 and τ_P for the atom number and band population and only τ_P for the double occupancy fraction and spin correlations (P_0 is then fixed to the initial value from the fit on all measured data points). We plot the mean standard deviation of the distribution of fitted parameters as shaded area in Fig. 3a-b and Fig. 4a,c and as asymmetric error bars in Fig. 3c-d and Fig. 4b.

Band transfer calculations

We calculate the band structure of our lattice and use the results to determine the expected population transfer between bands induced by the drive. We extend the methods described in Ref. [22] to 2D lattices. In brief, we start with the time-dependent Hamiltonian where we include the modulation as a periodic relative modulation of the lattice depth:

$$\mathcal{H} = \frac{\mathbf{p}^2}{2m} + V(x, y, z, \tau), \quad (\text{S4})$$

where the lattice potential is similar to Eq. S2. The modulation is implemented by multiplying the non-interfering lattice depth in x -direction with the time-dependent

waveform of the modulation:

$$V_{\overline{X}}(\tau) = V_{\overline{X}} \times (1 + A_{\omega} \sin(\omega\tau) + A_{2\omega} \sin(2\omega\tau + \varphi)). \quad (\text{S5})$$

The modulation in x -direction predominantly affects the dynamics in the xz -plane and we therefore neglect the y -direction in all subsequent calculations. To simplify further, we apply a coordinate transformation by rotating our frame by 45° :

$$x' = \frac{x+z}{\sqrt{2}} \quad z' = \frac{z-x}{\sqrt{2}} \quad (\text{S6})$$

The Bloch waves of the static Hamiltonian can be decomposed into their Fourier components:

$$\Psi_{q_{x'}, q_{z'}}^n(x', z') = \sum_{l, m=-\infty}^{+\infty} c_{l, m}^n(q_{x'}, q_{z'}) e^{i((2lk_L + q_{x'})x' + (2mk_L + q_{z'})z')}, \quad (\text{S7})$$

Expressing the Hamiltonian in the basis of these coefficients $c_{l, m}^n(q_{x'}, q_{z'})$ we can rewrite it to:

$$\mathcal{H}_{l, l', m, m'} = \begin{cases} \frac{\hbar^2}{2m} \left(2 \left(\frac{q_{x'}}{2} + lk_L \right)^2 + 2 \left(\frac{q_{z'}}{2} + mk_L \right)^2 \right) & \text{for } l = l' \text{ and } m = m' \\ -\frac{\alpha}{2} \sqrt{V_X V_Z} \cos(\phi) & \text{for } (|l - l'| = 1 \text{ and } m = m') \text{ or } (l = l' \text{ and } |m - m'| = 1) \\ -\frac{V_Z}{4} & \text{for } l = l' \pm 1 \text{ and } m = m' \pm 1 \\ -\frac{V_{\overline{X}}(\tau)}{4} - \frac{V_X}{4} e^{\pm i\theta} & \text{for } l = l' \pm 1 \text{ and } m = m' \mp 1 \\ 0 & \text{otherwise.} \end{cases} \quad (\text{S8})$$

We sample the positive quadrant of (q_x, q_z) in steps of $0.25 \times k_L$. For each q -vector we integrate the time-dependent Schrodinger equation for a finite number of evenly spaced steps in time up to a time $\Delta\tau$ which corresponds to the modulation time. We assume for the atoms to be initially in the lowest band and evolve that state in time. For each time step, we calculate the overlap of the time-evolved state with the static eigenstate of the ground band. The curves in Fig. 2a and Fig. 3 are obtained by taking the minimum overlap for each quasi-momentum and averaging over the entire Brillouin zone.

The Hubbard parameters t and U are numerically calculated from the Wannier functions of the lattice potential, which we obtain from band-projected position operators [31].